Journal of Zhejiang University-SCIENCE A (Applied Physics & Engineering) 2022 23(11):917-932
www.jzus.zju.edu.cn; www.springer.com/journal/11582
E-mail: jzus_a@zju.edu.cn

Research Article

https://doi.org/10.1631/jzus.A2200118

Check for updates

Frozen sand–concrete interface direct shear behavior under constant normal load and constant normal height boundary

Jian CHANG[1], Jian-kun LIU[1,2,3]✉, Ya-li LI[1]

[1]*School of Civil Engineering, Beijing Jiaotong University, Beijing 100044, China*
[2]*School of Civil Engineering, Sun Yat-sen University, Zhuhai 519082, China*
[3]*Southern Marine Science and Engineering Guangdong Laboratory (Zhuhai), Zhuhai 519082, China*

Abstract: The shear strength properties of the frozen sand–structure interface are critical for evaluating the serviceability of pile foundations in frozen ground. The shear characteristics of the frozen sand–concrete interface were studied with two boundary conditions (constant normal load (CNL) and constant normal height (CNH)), at three normal stresses (100, 200, and 300 kPa), and at three temperatures (−2, −5, and −8 ℃). A detailed comparative analysis was performed to explore the principal factors affecting the shear/normal-shear displacement. The results showed that the shear behavior of the frozen sand–concrete interface under CNL was similar to that under CNH. The shear stress–shear displacement exhibited strain softening. The temperature and normal stress were the major influences on normal properties. The lower the temperature and the higher the normal stress, the greater was the elastic shear modulus. The peak shear stress and critical shear stress exhibited a dependence on normal stress. An exponential growth in the peak shear stress was observed as the temperature decreased. Critical shear stress was dependent on temperature. The value and percentage of peak ice-cementation in peak shear stress was affected by temperature and normal stress.

Key words: Frozen sand–concrete interface; Peak shear strength; Critical shear strength; Ice-cementation; Boundary condition

1 Introduction

Understanding the mechanical properties of the soil–structure interface is important in geocryology engineering. The properties of the unfrozen soil–structure interface have been studied (de Gennaro and Frank, 2002; Lashkari, 2013; Saberi et al., 2018a). The influence of factors (such as normal stress, moisture content, roughness, and boundary conditions) on the soil–structure interface has been obtained. Particle image velocimetry (PIV) has been used to study the shear mechanical behavior of particles and their movements and shear bands have been observed directly (Peerun et al., 2019, 2020; Choo and Ong, 2020). In addition, the well-established four-stage soil shearing model was validated based on these studies. The advanced investigation method is of enormous significance for the study of the properties of the frozen interface (Wang et al., 2022). We have a thorough understanding of the shear mechanism of the unfrozen soil–structure interface based on these advanced studies. However, the serviceability of foundations in permafrost regions is determined by the mechanical properties of the frozen soil–structure interface, and investigating the influence of various factors on the soil–structure interface behavior can enable effective prediction of freezing strength, which can support structural design in permafrost regions.

Many investigations on the shear properties of frozen interfaces have been conducted. To acquire more accurate shear properties of frozen interfaces, researchers have conducted direct shear laboratory tests and pile foundation in-situ tests in permafrost regions. Numerical simulation methods have been designed to evaluate the shear strength of the frozen interface. It was found that the stress–strain behavior, strain rates, and freezing strength between frozen soil and structure are functions of the physical properties, loading rate, water content, and normal stress of soil according to direct shear laboratory tests; several methods to

✉ Jian-kun LIU, liujiank@mail.sysu.edu.cn
Jian CHANG, https://orcid.org/0000-0001-8481-4586

Received Mar. 9, 2022; Revision accepted July 21, 2022;
Crosschecked Sept. 23, 2022

predict the freezing bond strength have also been proposed (Roggensack and Morgenstern, 1978; Ladanyi, 1995; Ueda et al., 2004; Choi and Ko, 2011; Ko and Choi, 2011; Lee et al., 2013; Wen et al., 2013). The significance of water content, freezing temperature, and freezing time on the freezing strength of a frozen silty clay–concrete lining interface was analyzed. The results showed that the influence of freezing temperature is the most apparent among the three factors, and the effect of water content is the least (Sun et al., 2020). The shear characteristics of ice–frozen soil interface influenced by initial water content, initial void ratio, and negative temperature were investigated. Temperature and initial water content were found to be determinants of ice–frozen clay interface dilatancy and shear properties (Shi et al., 2020). The mechanical properties of a thawing soil–concrete interface influenced by moisture content, temperature, and normal load were analyzed (Pan et al., 2022). The stress path has a sensitive influence on rheological and stiffness properties based on a study of strength and deformation in frozen loess (Zhou et al., 2020). Model tests of pile foundations in permafrost regions have been conducted, and the freezing features of the pile–frozen soil interface and the relationship between the bearing capacity of a single pile and temperature have been acquired. The results indicated that the negative temperature is the determining factor for the pile foundation's bearing capacity. Also, the geotechnical frictional performance of piles in permafrost regions has been studied using model tests (Cheng et al., 2004; Wang et al., 2006). The shear and tensile strengths were positively correlated with negative temperature and moisture content based on the study, and a bond–friction interface model was built to predict the properties of pile–frozen soil (Sun et al., 2021). The shear properties were examined according to negative temperature direct shear tests and the deformation mechanism of the warm frozen silt–cemented soil interface by a binary medium model (Zhang et al., 2021). The freezing strength of a frozen sand–steel plate interface was analyzed based on tests, and a damage model was proposed based on the comprehensive continuous damage theory and the statistical strength theory (Shi and Yang, 2021). A series of pile foundation in-situ tests showed that the shearing deformation of frozen soil around the pile and the changes in porosity in the soil structure resulted in particularly low pile uplift capacities, and the friction coefficient played an important role in the growth of freezing strength (Biggar and Sego, 1993; Zhang et al., 2008; de Hollanda Cavalcanti Tsuha et al., 2016; Ji et al., 2017). Low temperature decreased the shear strength of pile-frozen soil based on the study, and a friction parameter was suggested to describe the resistance of the interface (Aldaeef and Rayhani, 2021). The freezing shear tests on frozen sand–steel pipe interfaces were performed, and a judgement equation ($\tau_{as,i}-\sigma_{as,i}\leqslant 0$, where $\tau_{as,i}$ is the frozen shear strength, and $\sigma_{as,i}$ is the frozen shear stress) for freezing shear failure was proposed (Sumitani et al., 2007). The judgement equation illustrated the strength failure condition of the frozen sand–steel pipe interfaces. Sumitani et al. (2007) divided the boundary curve of a frozen interface into several segments and found that a shear strength failure of frozen sand steel pipe interfaces would happen when the load along the micro-segment was smaller than the shear stress of the micro-segment. Numerical simulation methods of pile interaction with frozen soil have been established to analyze heat transfer, soil compression, thaw consolidation, and embankment deformation (Puswewala, 1991; Chen et al., 2022).

Most tests were conducted under a constant normal load (CNL) because of restrictions in the test equipment and engineering conditions. The different boundary conditions exhibit different soil–structure interfaces, which impose different stress paths. Results showed that the load transfer mechanism, shear and volumetric behavior of the interface predominantly depend on the stress path (Johnston et al., 1987; Tabucanon et al., 1995; Evgin and Fakharian, 1996; Fakharian, 1996; DeJong et al., 2003; Mortara et al., 2007). Hence, it is essential to study the shear properties of interfaces under complex boundary conditions (CNL, constant normal height (CNH), and constant normal stiffness (CNS)) in permafrost regions to provide theoretical and experimental support for structural design (Saberi et al., 2018b).

Analysis of the development of shear strength and displacement/stress–shear displacement under different boundary conditions is helpful to understanding the shear properties and mechanism of a frozen interface. This study investigates the development of shear strength, ice-cementation, and displacement/stress–shear displacement of sand–concrete interfaces through a series of experiments using a self-developed large-scale

direct shear apparatus at Beijing Jiaotong University, China and considering different temperatures, normal stresses, and boundary conditions. Section 2 provides a detailed description of the testing process. In Section 3, the influence of normal stress, temperature, and boundary conditions on stress/displacement–shear displacement and shear strength are analyzed. Finally, Section 4 presents the conclusions of the study. The main findings of this study can assist in understanding the bearing capacity mechanism of temperature-controlled thermal piles working in high-speed railways in permafrost regions and provide data support for establishing a constitutive model of frozen sand–concrete interfaces under shear loading.

2 Experimental scheme and testing process

The study of shear behavior influenced by normal stress, temperature, and boundary conditions was investigated in a series of frozen sand interface direct shear tests. The specimen preparation and test procedures are explained as follows.

2.1 Testing apparatus

The large-scale direct shear test apparatus used for the frozen sand–concrete interface was developed at Beijing Jiaotong University, China (Chang et al., 2022). The walls of the shear boxes were hollow and connected with a refrigeration system by four tubes with the coolant circulated within the walls of the shear boxes to control their inner environmental temperature. The temperature could be held constant or varied within the range of −25 to 30 ℃ by program control of the refrigeration system. The schematic of the specimen in the shear boxes is shown in Fig. 1.

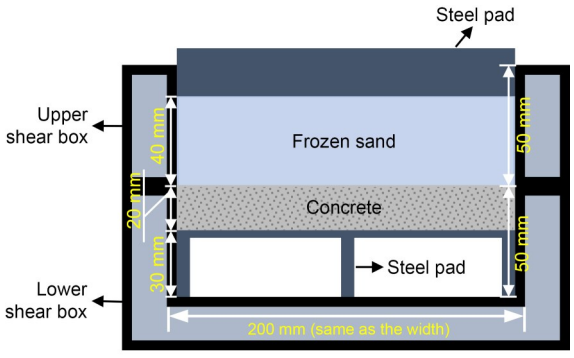

Fig. 1 Schematic view of the specimen in shear boxes

2.2 Material and specimen preparation

The soil used for specimens was poorly graded fine sand (based on the unified soil classification system) according to the physical properties of sand as presented in Table 1. The grain size distribution of sand is presented in Fig. 2. The maximum dry density and optimum water content were 1.62 g/cm^3 and 18%, respectively, based on the ASTM Standards.

Table 1 Physical properties of the sand

Parameter		Value
Constrained grain size, d_{60} (mm)		0.195
Median grain size, d_{30} (mm)		0.129
Effective grain size, d_{10} (mm)		0.095
Maximum dry density (g/cm^3)		1.620
Optimum water content (%)		18.00
Grain size distribution (%)	<2.000 mm	99.25
	<0.500 mm	96.95
	<0.250 mm	80.07
	<0.075 mm	6.00

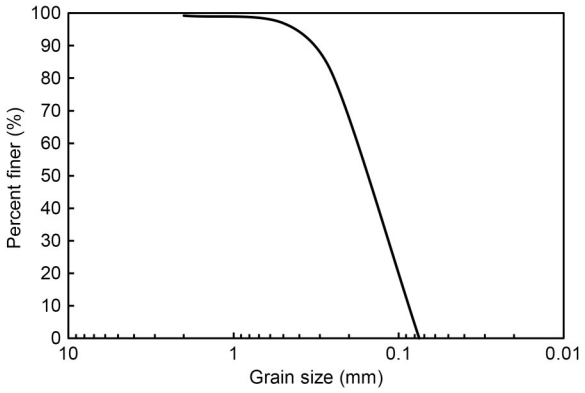

Fig. 2 Grain size distribution of sand

The artificial frozen sand–concrete interface specimens are prepared in three steps (Chang et al., 2022): sand sample preparation, concrete specimen preparation, and frozen saturated sand–concrete specimen preparation.

2.3 Testing procedure

Direct shear tests were controlled by horizontal displacement, and the shear rate was 0.5 mm/min. Based on the restriction of the performance of the large-scale direct shear apparatus, these tests were conducted under CNL and CNH. The temperatures

were −2, −5, and −8 °C, and the normal stresses were 100, 200, and 300 kPa. The normal stiffness of the interface constraints was zero (Fig. 3a) when the specimen was under CNL, and the normal stiffness was infinite (Fig. 3b) when the specimen was under CNH. The normal stress was imposed after placing the specimen in the pre-cooling shear boxes, keeping the normal stress throughout the test under CNL and fixing the height throughout the test under CNH. The loading processes of the frozen sand–concrete interface are illustrated in Fig. 4. The normal stress σ_n under CNL kept constant during shear progress ($\sigma_n=\sigma_n^i$, where σ_n^i is the initial normal stress), and the normal stress σ_n under CNH kept changing during shear progress. The stress–shear displacement curve after the peak shear stress was steady, which indicated the end of the shearing process. Each test was repeated three times, and the results were averaged.

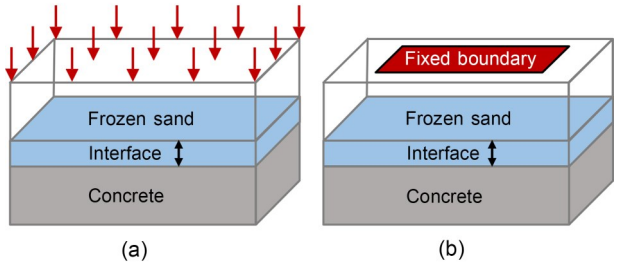

Fig. 3 Schematic view of normal stiffnesses of the frozen sand–concrete interface under CNL and CNH: (a) zero normal stiffness (CNL); (b) infinite normal stiffness (CNH)

3 Results and discussion

3.1 Shear stress–shear displacement properties

The feature points of the shear stress–shear displacement curve were introduced to comprehensively study the shear characteristics, as shown in Fig. 5. When the shear stress increased to the first point, the volume of the frozen interface began to increase, and that stress point was defined as the dilatancy stress. The second point, at the peak of the curve, was defined as the peak shear stress, τ_p, and the corresponding shear displacement was defined as the peak shear displacement, u_p. The shear stress then gradually tended towards a stable value as the shear displacement increased, and that stable shear stress was defined as the critical shear stress, τ_c.

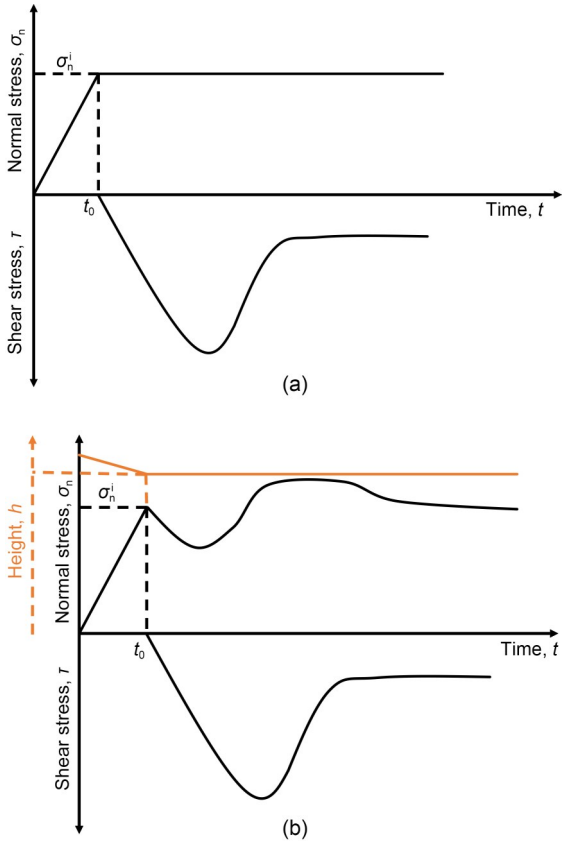

Fig. 4 Schematic view of loading processes of the frozen sand–concrete interface: (a) CNL; (b) CNH. t_0 is the time the initial normal stress reached the design value

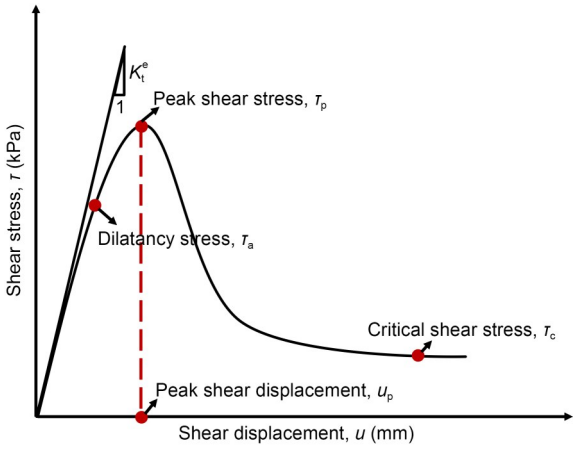

Fig. 5 Schematic of characteristic points in a shear stress–shear displacement curve. K_t^e is the elastic shear modulus

The shear stress–shear displacement relationships at different temperatures (T) and different normal stresses under CNL and CNH are shown in Figs. 6 and 7, respectively.

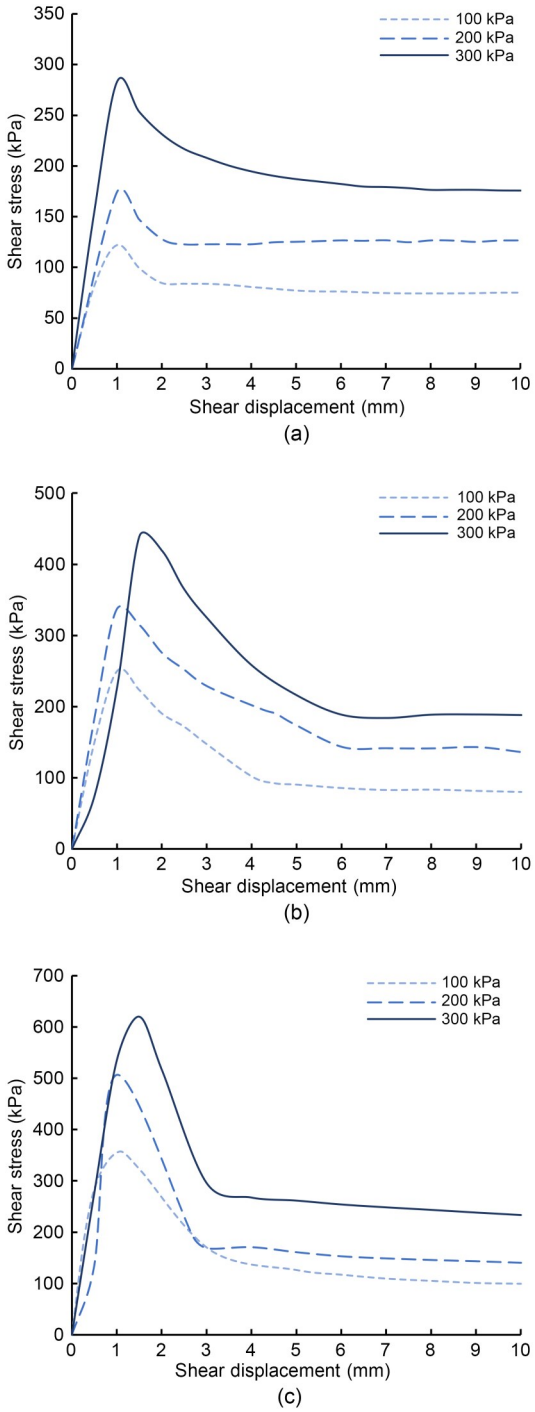

Fig. 6 Shear stress–shear displacement curves at different normal stresses under CNL: (a) T=−2 ℃; (b) T=−5 ℃; (c) T=−8 ℃

3.1.1 Influence of normal stress

The degree of strain softening was obvious. τ_p and τ_c of the frozen sand–concrete interface were affected by the normal stress.

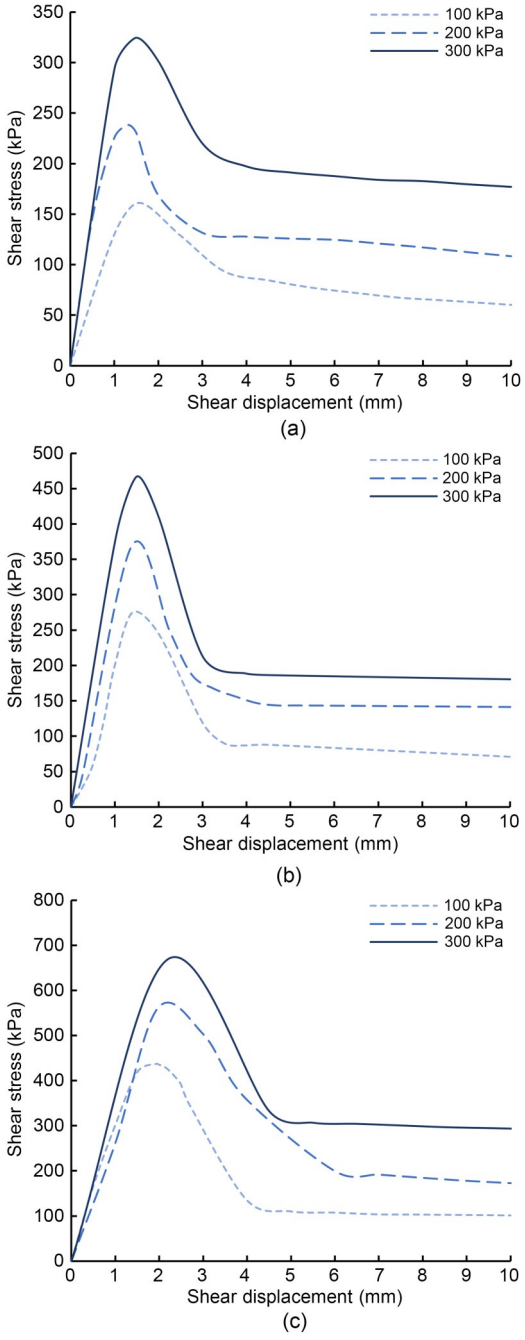

Fig. 7 Shear stress–shear displacement curves at different normal stresses under CNH: (a) T=−2 ℃; (b) T=−5 ℃; (c) T=−8 ℃

3.1.2 Influence of temperature

The shear stress–shear displacement relationships at different negative temperatures were similar, but τ_p and τ_c were different. The shear stress–shear displacement relationship tended to soften obviously at the negative temperature under both boundary conditions,

as shown in Figs. 6 and 7. The degree of strain-softening increases with decreasing temperature. There was a brittle failure after up and the shear stress reduced after τ_p.

3.1.3 Influence of boundary conditions

The development trends of shear stress–shear displacement under CNL and CNH are similar, as presented in Figs. 6 and 7.

3.2 Normal displacement/stress–shear displacement properties

Research on the normal displacement–shear displacement relationship under CNL and the normal stress–shear displacement relationship under CNH has improved the understanding of the mechanical characteristics of the sand–concrete interface. The schematic of normal and shear displacements of the frozen interface is illustrated in Fig. 8, taking increasing normal displacement as compression. The normal displacement of the frozen interface under CNL is less than 0.7 mm based on the tests (Fig. 9), which make it difficult to measure. In addition, higher precision displacement sensor is needed due to the small magnitude of the normal displacement of the frozen interface. The development of normal displacement with shear displacement showed a compression trend in this study. The reasons for that may be that the total normal displacement of frozen sand in the shear box was measured or the precision of the displacement sensor was insufficient. Therefore, it is necessary to investigate the development of the normal stress of the frozen interface under CNH to gain further information.

The feature points on the relation curves of normal stress–shear displacement under CNH are shown in Fig. 10. The normal stress decreases to a valley with increasing shear displacement, then increases to peak normal stress, σ_p, and remains constant, before finally decreasing and tending towards stability. In this process, the decrease in the normal stress indicates the compression trend of the sand–concrete interface, and the increase after the valley indicates the dilatancy trend of the sand–concrete interface. This study set the valley point as the phase transition point, σ_t, and the normal stress increased with increasing shear displacement until σ_p. The shear displacement was equal to or greater than u_p when the normal stress peaked in reference to the corresponding shear stress–shear displacement curve. It was found that when the normal stress remained constant at the peak, the shear stress decreased, and when the normal stress was in a stable state, the shear stress entered its residual state in reference to the corresponding shear stress–shear displacement curve (Fig. 5). In this study, the normal stress stable and shear stress residual states under CNH were assumed to be a critical state.

3.2.1 Influence of initial normal stress

The influence of initial normal stress on normal stress–shear displacement relationship under CNH was investigated, as shown in Fig. 11. The feature points of the normal stress–shear displacement curve were more apparent with higher initial normal stress at different temperatures. σ_t, σ_p, slip stage, and stable stage of the normal stress–shear displacement curve appeared with higher initial normal stress. The normal stress–shear displacement curve developed with a gentle

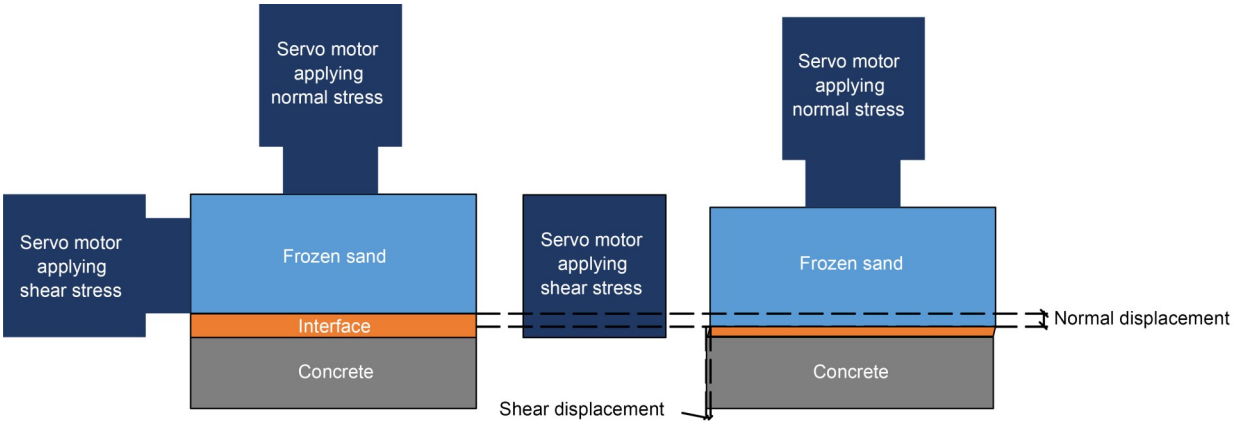

Fig. 8 Schematic of normal displacement of the frozen interface

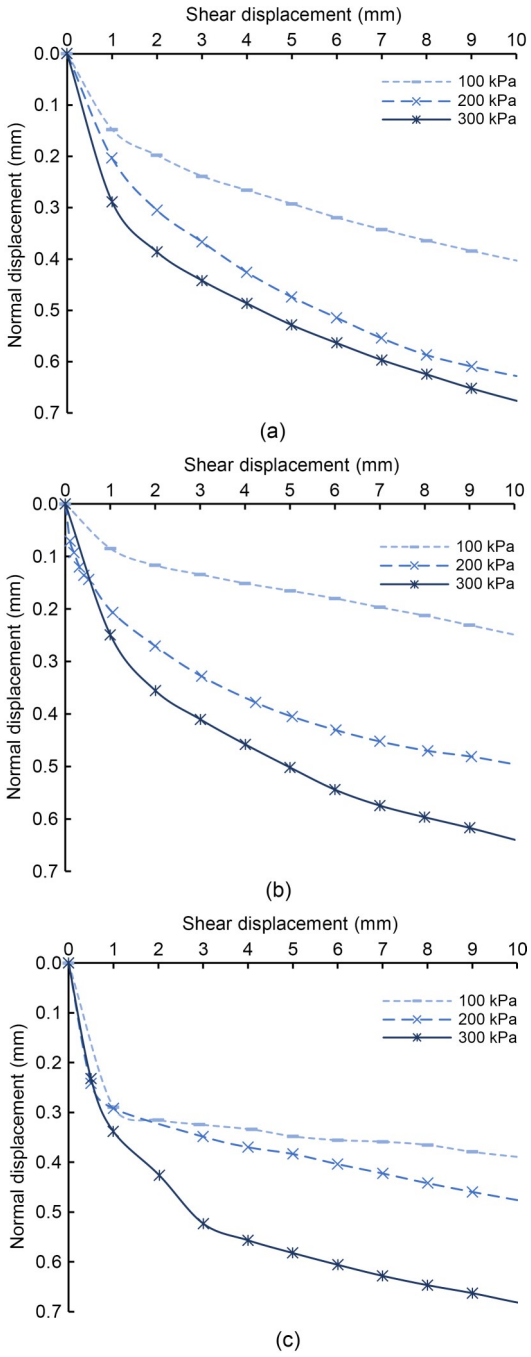

Fig. 9 Normal displacement–shear displacement curves of the sand–concrete interface under CNL: (a) T=−2 ℃; (b) T=−5 ℃; (c) T=−8 ℃

slope and some feature points disappeared under lower initial normal stress. σ_t and σ_p increased when initial normal stress was increasing at different temperatures. The absolute difference between σ_t and σ_n^i increased with increasing initial normal stress at different temperatures. The absolute difference between σ_p and σ_n^i at −8 ℃ increased, with increasing initial normal stress, as illustrated in Fig. 11c. As for −8 ℃, the absolute difference between σ_t and σ_n^i was 8.75, 9.75, and 17.63 kPa and the absolute difference between σ_p and σ_n^i was 73.13, 78.38, and 75.75 kPa when the initial normal stresses were 100, 200, and 300 kPa, respectively.

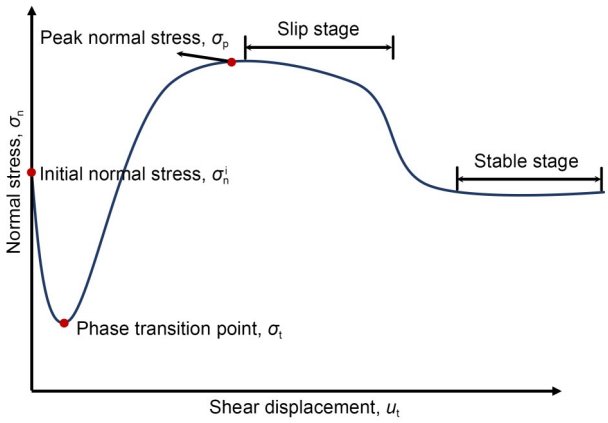

Fig. 10 Schematic of characteristic points in a normal stress–shear displacement curve

3.2.2 Influence of temperature

The temperature had an appreciable effect on the normal stress under CNH. σ_n^i=100 kPa was used as an example to illustrate the influence of temperature on the normal stress–shear displacement relationship. The normal stress–shear displacement curve at −2 ℃ was relatively flat (Fig. 12a), and the normal stress decreased with increasing shear displacement to σ_t and remained constant. An undulating curve of normal stress with shear displacement at −5 ℃ is shown in Fig. 12a. The normal stress decreased with increasing shear displacement until σ_t, then increased to σ_p and declined, and finally decreased to a stable state. A curve of the normal stress–shear displacement relationship at −8 ℃ is shown in Fig. 12a. As shear displacement increased, the normal stress decreased to σ_t, then increased to σ_p, and dropped to a stable state. Moreover, σ_p depended on the temperature. The variation of σ_p at σ_n^i=100 kPa is shown in Fig. 12a. σ_p at −2 ℃ was 128.0 kPa, σ_p at −5 ℃ was nearly 160.0 kPa, and σ_p at −8 ℃ was 172.2 kPa. σ_t increased with decreasing temperature. σ_t was 85.5, 86.5, and 90.5 kPa when the temperature was −2, −5, and −8 ℃, respectively.

3.3 Elastic shear modulus properties K_t^e

The shear stress–shear displacement curves of the frozen sand–concrete interface under CNL, at

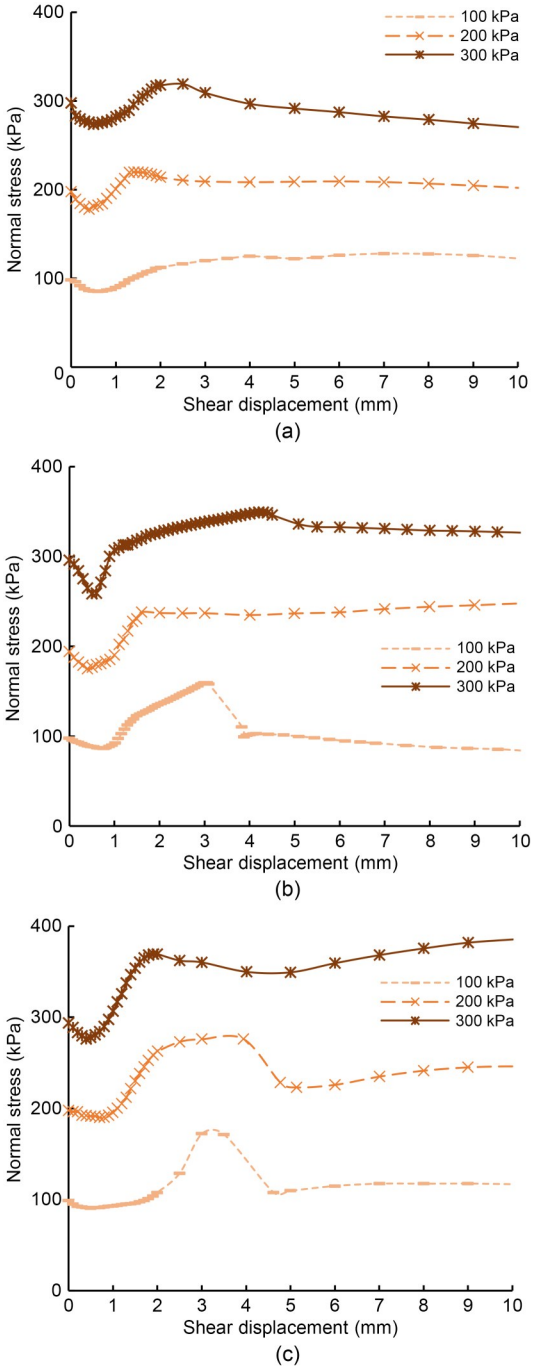

Fig. 11 Normal stress–shear displacement curves of sand–concrete interface under CNH: (a) T=−2 ℃; (b) T=−5 ℃; (c) T=−8 ℃

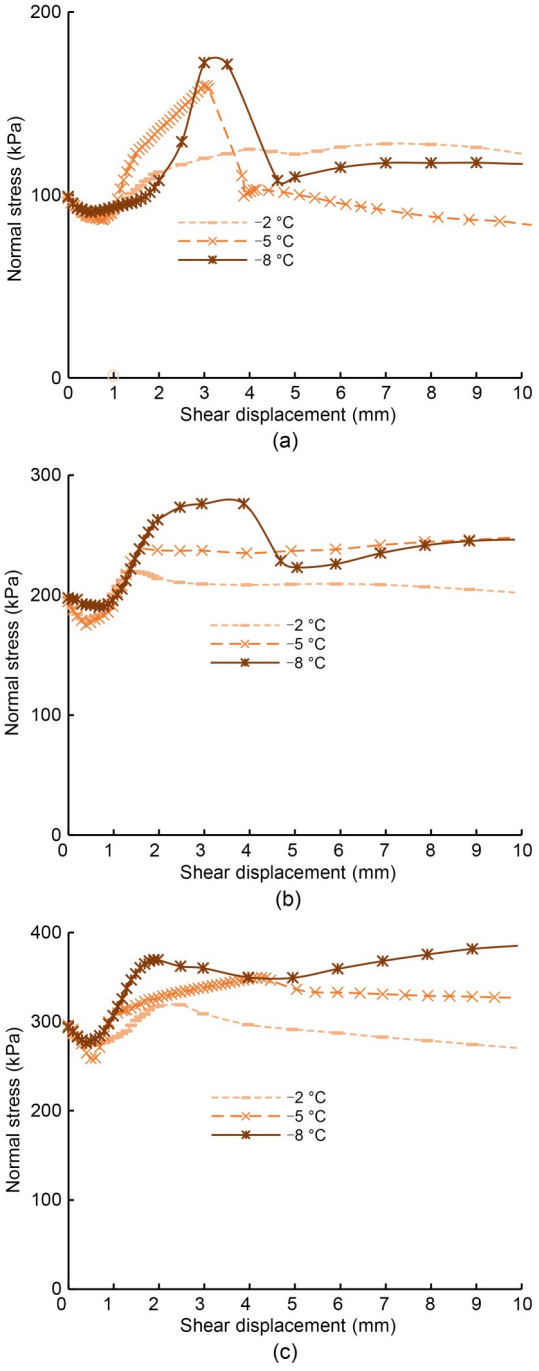

Fig. 12 Normal stress–shear displacement curves of the sand–concrete interface under CNH: (a) 100 kPa; (b) 200 kPa; (c) 300 kPa

different temperatures and normal stresses, are shown in Fig. 6. The elastic shear modulus is the tangential slope of the initial stage of the shear stress–shear displacement curve under CNL and CNS boundary conditions (Lashkari, 2013), as shown as Fig. 5. The elastic shear modulus reflects the elastic properties of the frozen sand–concrete interface. The elastic shear properties of the frozen sand–concrete interface were studied based on the monotonic shear tests with different temperatures and normal stresses.

The effects of initial normal stress on K_t^e were studied, as illustrated in Fig. 13. K_t^e increased linearly

with increasing initial normal stress and decreasing temperature. The increment of elastic shear modulus increased with increasing initial normal stress and decreased with decreasing temperature. The relationship between initial normal stress and elastic shear modulus can be described by the function $K_t^e=f(\sigma_n, T)=a(T)\sigma_n+m(T)$ based on the results of experiments, where a and m are fitting parameters.

Further study of the influence of temperature on the elastic shear modulus is shown in Fig. 14. As the temperature decreased, the value of parameter a decreased, and the value of parameter m increased. Parameters a and m could be calculated by empirical formulas as follows:

$$a(T)=0.01T+0.17, \quad (1)$$

$$m(T)=-12.09T-9.94. \quad (2)$$

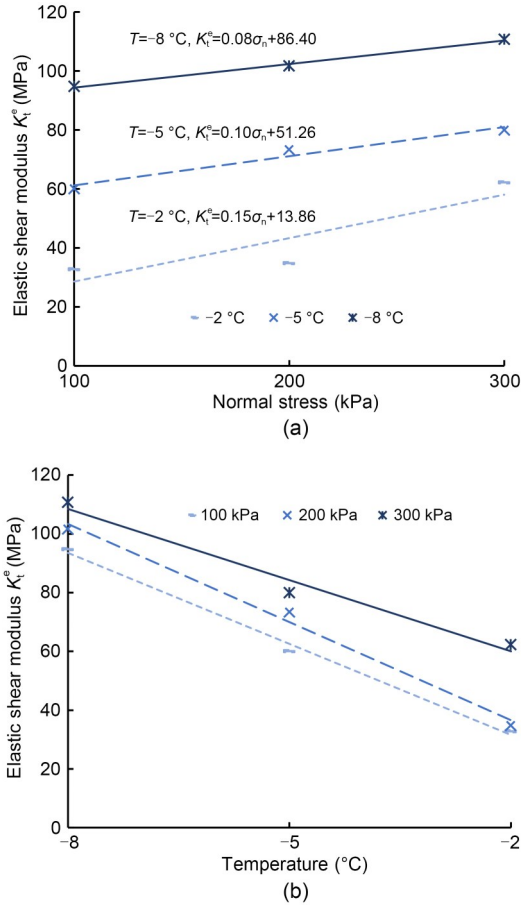

Fig. 13 Elastic shear modulus of the frozen sand–concrete interface: (a) relationship between elastic shear modulus and normal stress; (b) relationship between elastic shear modulus and temperature

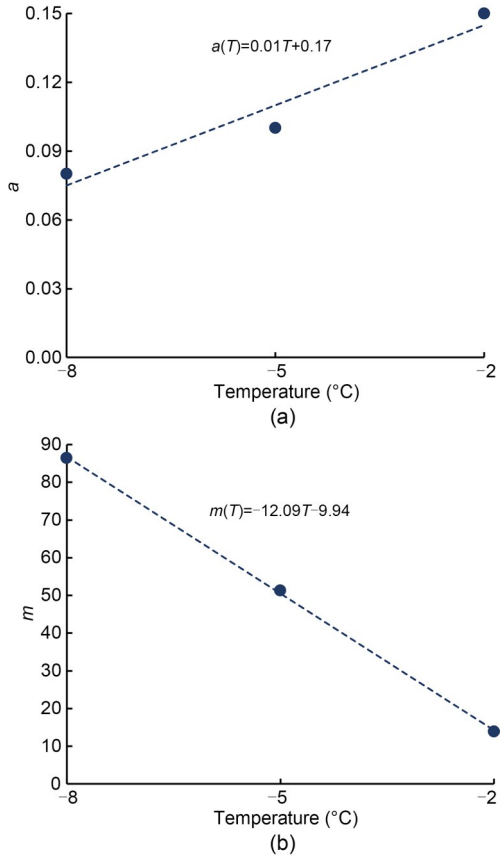

Fig. 14 Parameters *a* (a) and *m* (b) with temperature

3.4 Shear strength properties

The shear band of frozen sand–structure interface consists of sand particles, ice, unfrozen water, and gas. The cementation produced by ice crystals is the major contribution to the shear strength of the frozen interface. The term "ice-cementation" is used here.

3.4.1 Influence of normal stress

Figs. 15 and 16 illustrate the relationships of τ_p-σ_n and τ_c-σ_n at different temperatures, under CNL and CNH, respectively. τ_p and τ_c showed a linearly increasing trend with increasing normal stress at a certain temperature under both boundary conditions. The relationships of τ_p-σ_n and τ_c-σ_n can be described by the Mohr-Coulomb failure criterion $\tau=\sigma_n\tan\varphi+c$ (parameters $\tan\varphi$ and c are the friciton coefficient and cohesion, respectively), as shown in Figs. 15 and 16.

3.4.2 Influence of temperature

Further studies were conducted to investigate factors affecting the cohesion c and friction coefficient

tanφ of the Mohr-Coulomb failure criterion $\tau=\sigma_n\tan\varphi+c$. The cohesion c and friction coefficient tanφ of τ_p and τ_c at different temperatures under CNL and CNH are listed in Tables 2 and 3, respectively. The cohesion c of τ_p increased significantly, while that of τ_c varied slightly with the decrease in temperatures under both boundary conditions, as shown in Tables 2 and 3. The relationships c-T of τ_p could be fitted by an exponential function $c_p^{CNL}=20.09e^{-0.33T}$ under CNL and $c_p^{CNH}=45.49e^{-0.26T}$ under CNH. For simplicity, the influences

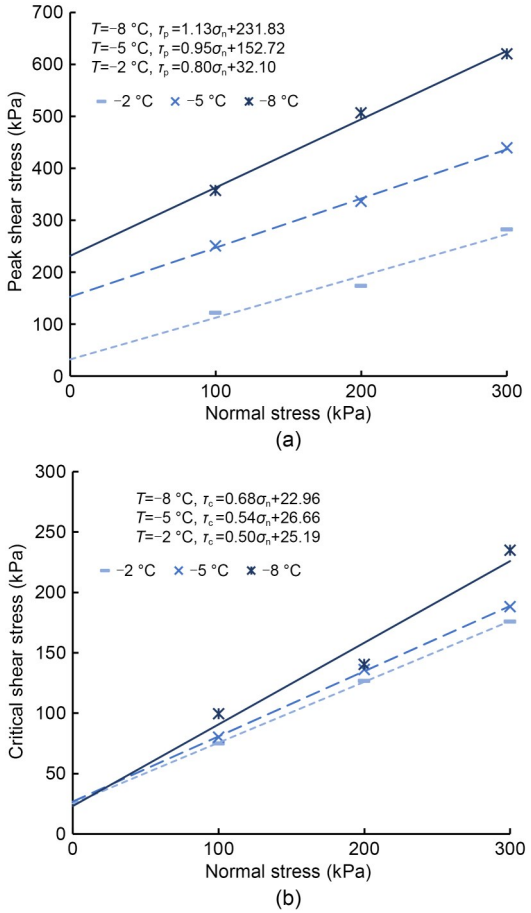

Fig. 15 Shear strength of the sand–concrete interface under CNL: (a) peak shear stress; (b) critical shear stress

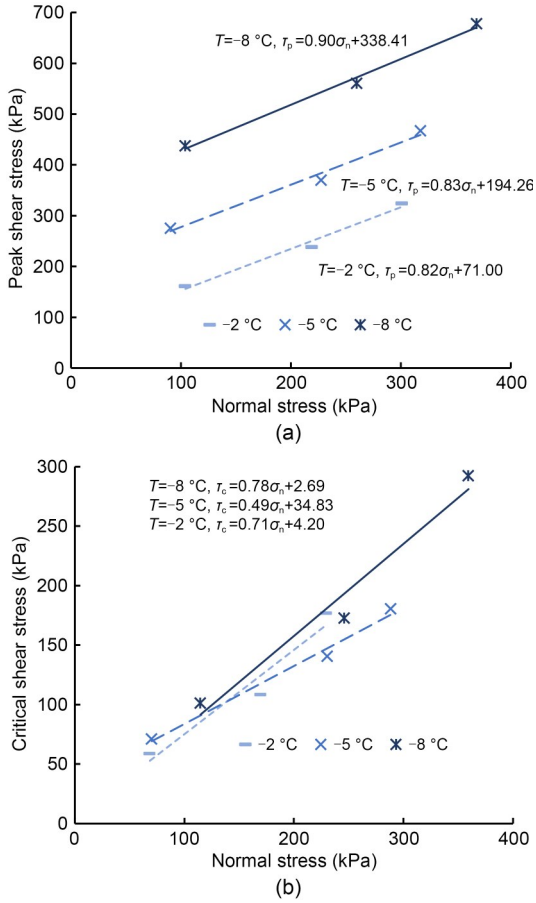

Fig. 16 Shear strength of the sand–concrete interface under CNH: (a) peak shear stress; (b) critical shear stress

Table 2 Parameters of the interface under CNL

Temperature (°C)	Cohesion (kPa)		Friction coefficient	
	Peak shear stress	Critical shear stress	Peak shear stress	Critical shear stress
−2	32.10	25.19	0.80	0.50
−5	152.72	26.66	0.95	0.54
−8	231.83	22.96	1.31	0.68

Table 3 Parameters of the interface under CNH

Temperature (°C)	Cohesion (kPa)		Friction coefficient	
	Peak shear stress	Critical shear stress	Peak shear stress	Critical shear stress
−2	71.00	2.69	0.82	0.71
−5	194.26	34.83	0.83	0.49
−8	338.41	4.20	0.90	0.78

of temperature on the friction coefficient tanφ of τ_p and the cohesion c of τ_c were ignored. Then, the weighted average method was adopted to obtain the friction coefficient tanφ of τ_p and the cohesion c of τ_c under both boundary conditions (Ladanyi, 1995). The relationship between the friction coefficient tanφ and temperature of τ_c under both boundary conditions is shown in Fig. 17. The parameter tanφ increased with decreasing temperature under both boundary conditions. All the parameters were taken into the Mohr-Coulomb failure criterion. The equations for τ_p with initial normal stress and temperature, as well as τ_c with initial normal stress and temperature, were obtained, as follows:

$$\tau_p^{CNL} = 1.02\sigma_n + 20.09e^{-0.33T}, \quad (3)$$

$$\tau_c^{CNL} = (-0.03T + 0.42)\sigma_n + 24.94, \quad (4)$$

$$\tau_p^{CNH} = 0.85\sigma_n + 45.49e^{-0.26T}, \quad (5)$$

$$\tau_c^{CNH} = (-0.01T + 0.60)\sigma_n + 13.91. \quad (6)$$

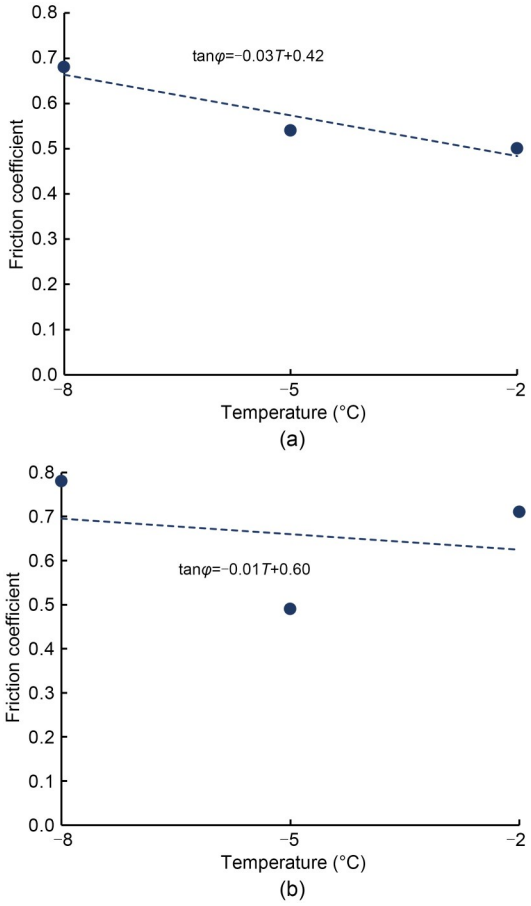

Fig. 17 Relationship of the friction coefficient to temperature: (a) CNL; (b) CNH

The variations in τ_p and τ_c of the sand–concrete interface with temperature under CNL and CNH are illustrated in Figs. 18 and 19, respectively. There was a significant exponential increase in τ_p of the sand–concrete interface with decreasing temperature at the same normal stress under CNL and CNH, as illustrated in Figs. 18a and 19a, which is consistent with the exponential relationship τ_p-T derived from the Mohr-Coulomb failure criterion from the first part of Section 3.4.2. Lower temperature caused higher τ_c at a particular normal stress under CNL and CNH, as shown in Figs. 18b and 19b.

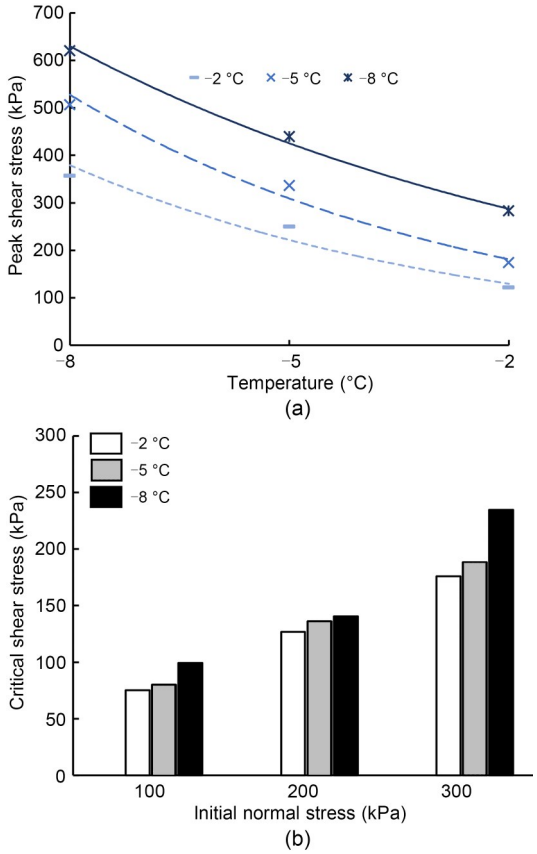

Fig. 18 Shear strength of sand–concrete interface under CNL: (a) peak shear stress; (b) critical shear stress

The characteristics of shear stress were comprehensively analyzed and combined with the above. The shear stress increased with increasing shear displacement when the shear displacement was less than u_p ($u<u_p$). Subsequently, it reached τ_p while the shear displacement was u_p ($u=u_p$), as shown in Fig. 6. The shear stress decreased when the shear displacement increased over u_p ($u>u_p$). Thus, brittle failure of ice-cementation occurred when the shear

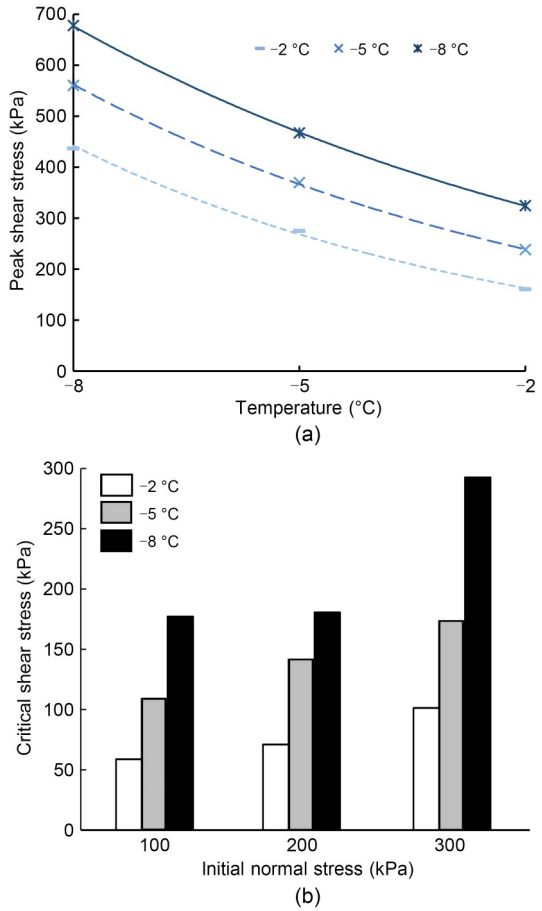

Fig. 19 Shear strength of sand–concrete interface under CNH: (a) peak shear stress; (b) critical shear stress

displacement exceeded u_p. Thereafter, the shear displacement continued to increase, and the shear stress gradually trended towards τ_c.

The ice-cementation was analyzed based on the calculation method suggested by He et al. (2018). The peak ice-cementation was the difference between τ_p and τ_c, as $\tau_p^i = \tau_p - \tau_c$, for CNL and CNH, as shown in Tables 4 and 5, respectively. The calculations from Tables 4 and 5 show that there was a significant increase in τ_p^i with decreasing temperature and increasing normal stress. A comparison of the percentage of peak ice-cementation at peak shear stress under different initial normal stresses at −2, −5, and −8 °C is shown in Fig. 20. The percentage of peak ice-cementation at peak shear stress decreased with increasing initial normal stress, as shown in Fig. 20. The interaction of sand particles increased with increasing initial normal stress and then the shear strength of sand increased. This showed that the shear strength of sand played a major role with increasing initial normal stress in the peak shear stress of the frozen interface. The value and percentage of peak ice-cementation in the peak shear stress increased with decreasing temperature. This is because ice-cementation was determined by the ice film thickness, which caused a higher value and percentage of peak ice-cementation in the peak shear stress with decreasing temperature (Volokhov, 2003). Thus, there was an increase in the shear stress with decreasing temperature before the shear displacement reached u_p (before the failure of ice-cementation).

3.4.3 Influence of boundary conditions

The influence of different boundary conditions (CNL and CNH) on τ_p^i, τ_p, and τ_c is shown in Fig. 21. τ_p^i under CNH was higher than that under CNL at the same temperature and initial normal stress, as shown in Fig. 21a. The percentage of peak ice-cementation in the peak shear stress was higher under CNH, as illustrated in Fig. 20. τ_p was affected by the negative temperature and initial normal stress under both

Table 4 Peak ice-cementation of the frozen sand–concrete interface under CNL

Temperature (°C)	Initial normal stress (kPa)	Peak ice-cementation τ_p^i (kPa)	Percentage of peak ice-cementation in peak shear stress τ_p^i/τ_p (%)
−2	100	46.95	38.48
	200	49.90	28.71
	300	107.03	37.84
−5	100	170.13	68.00
	200	199.98	59.52
	300	251.15	57.17
−8	100	257.78	77.15
	200	366.03	72.28
	300	385.25	62.14

Table 5 Peak ice-cementation of the frozen sand–concrete interface under CNH

Temperature (°C)	Initial normal stress (kPa)	Peak ice-cementation τ_p^i (kPa)	Percentage of peak ice-cementation in peak shear stress τ_p^i/τ_p (%)
−2	100	102.38	63.54
	200	129.93	54.54
	300	147.55	45.47
−5	100	204.23	74.24
	200	208.93	61.95
	300	256.78	61.38
−8	100	329.63	76.83
	200	387.48	69.17
	300	375.28	56.85

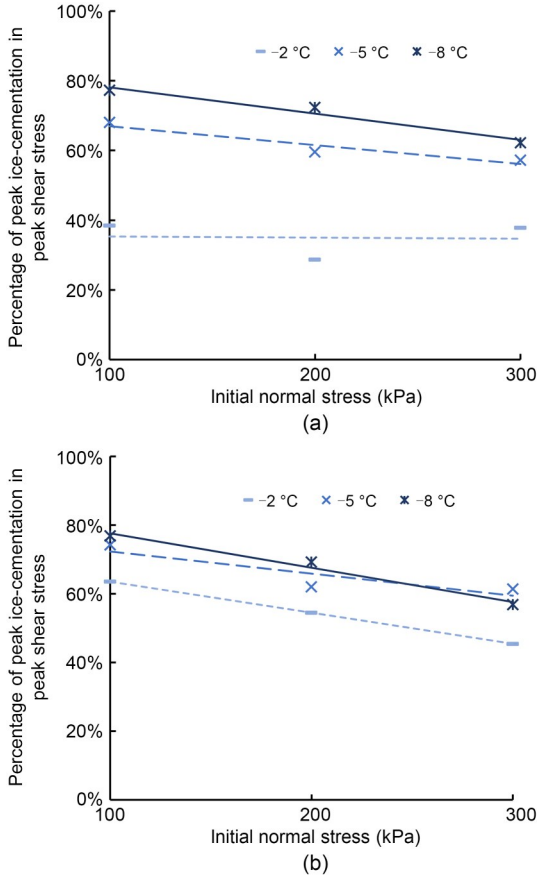

Fig. 20 Peak ice-cementation of the frozen sand–concrete interface: (a) CNL; (b) CNH

boundary conditions, and τ_p under CNH was higher at the same temperature and initial normal stress, as shown in Fig. 21b. Dilation occurs with increasing shear displacement for shear displacements less than u_p (Fig. 11). Dilatancy caused a higher normal stress under CNH, which implies higher ice-cementation and higher peak shear stress. τ_c under CNH was lower at

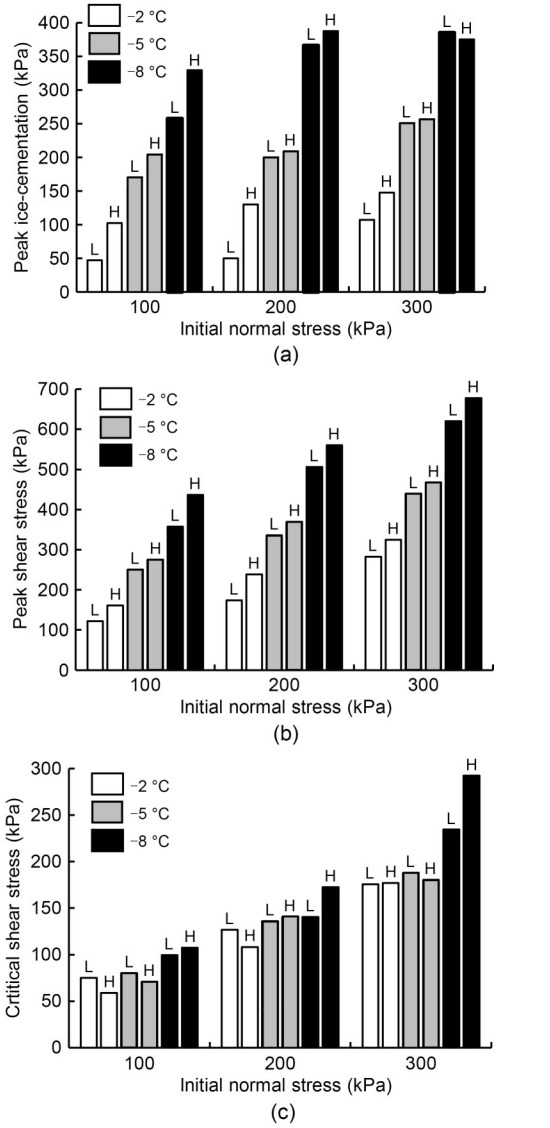

Fig. 21 Comparison of shear strength under CNL (L) and CNH (H): (a) peak ice-cementation; (b) peak shear stress; (c) critical shear stress

the same temperature and initial normal stress, as shown in Fig. 21c. The compression occurred with increasing shear displacement at the residual stage, which led to a decreasing normal stress under CNH. It implied that τ_c continued to decrease. However, the normal stress remained constant under CNL, which caused a higher critical shear stress.

4 Conclusions

The shear properties and influencing factors on the frozen sand–concrete interface were investigated through a series of large-scale direct shear tests at different temperatures, normal stresses, and boundary conditions (including CNL and CNH). The results can be summarised as follows:

(1) The development trends of shear stress–shear displacement under CNL and CNH were similar. The shear stress–shear displacement relationship displayed a significant softening at negative temperatures. Lower temperature and higher normal stress resulted in an increasing degree of strain softening.

(2) The normal stress–shear displacement relationship under CNH was dependent on the initial normal stress and temperature. The feature points were more apparent with higher initial normal stress and lower temperature.

(3) The elastic shear modulus showed a linear increase with decreasing temperature and increasing initial normal stress.

(4) The peak shear stress and critical shear stress showed a linearly increasing trend with increasing initial normal stress, which could be described by the Mohr-Coulomb failure criterion under CNL and CNH. The temperature had an appreciable effect on the cohesion of the peak shear stress and the friction coefficient of the critical shear stress.

(5) Under CNL and CNH, the value and percentage of peak ice-cementation in peak shear stress increased with decreasing temperature. The value of peak ice-cementation increased with increasing initial normal stress. Nevertheless, the percentage of peak ice-cementation in peak shear stress decreased with the increase in initial normal stress.

(6) The peak shear stress and ice-cementation were higher, and the critical shear stress was lower under CNH than those under CNL.

Acknowledgments

This work is supported by the National Natural Science Foundation of China (No. 41731281) and the Key Foundation of Guangdong Province (No. 2020B1515120083), China.

Author contributions

Jian CHANG and Jian-kun LIU designed the research. Jian CHANG and Ya-li LI processed the corresponding data. Jian CHANG wrote the first draft of the manuscript. Ya-li LI helped to organize the manuscript. Jian CHANG revised and edited the final version.

Conflict of interest

Jian CHANG, Jian-kun LIU, and Ya-li LI declare that they have no conflict of interest.

References

Aldaeef AA, Rayhani MT, 2021. Pile-soil interface characteristics in ice-poor frozen ground under varying exposure temperature. *Cold Regions Science and Technology*, 191: 103377. https://doi.org/10.1016/j.coldregions.2021.103377

Biggar KW, Sego DC, 1993. Field pile load tests in saline permafrost. I. Test procedures and results. *Canadian Geotechnical Journal*, 30(1):34-45. https://doi.org/10.1139/t93-004.

Chang J, Liu JK, Li YL, et al., 2022. Elastoplastic behavior of frozen sand–concrete interfaces under cyclic shear loading. *Journal of Zhejiang University-SCIENCE A (Applied Physics & Engineering)*, 23(9):683-703. https://doi.org/10.1631/jzus.A2100667

Chen WH, Luo Q, Liu JK, et al., 2022. Modeling of frozen soil-structure interface shear behavior by supervised deep learning. *Cold Regions Science and Technology*, 200: 103589. https://doi.org/10.1016/j.coldregions.2022.103589

Cheng YF, Lu XL, Liu HQ, et al., 2004. Model test study on pile foundation of 110 kV transmission line of Qinghai-Tibet railway in frozen soils. *Chinese Journal of Rock Mechanics and Engineering*, 23(S1):4378-4382 (in Chinese). https://doi.org/10.3321/j.issn:1000-6915.2004.z1.022

Choi CH, Ko SG, 2011. A study for predicting adfreeze bond strength from shear strength of frozen soil. *Journal of the Korean Geotechnical Society*, 27(10):13-23. https://doi.org/10.7843/kgs.2011.27.10.013.

Choo CS, Ong DEL, 2020. Assessment of non-linear rock strength parameters for the estimation of pipe-jacking forces. Part 2. Numerical modeling. *Engineering Geology*, 265:105405. https://doi.org/10.1016/j.enggeo.2019.105405

de Gennaro V, Frank R, 2002. Elasto-plastic analysis of the interface behaviour between granular media and structure. *Computers and Geotechnics*, 29(7):547-572. https://doi.org/10.1016/S0266-352X(02)00010-1

de Hollanda Cavalcanti Tsuha C, dos Santos Filho JMSM, da Costa Santos T, 2016. Helical piles in unsaturated

structured soil: a case study. *Canadian Geotechnical Journal*, 53(1):103-117. https://doi.org/10.1139/cgj-2015-0017

DeJong JT, Randolph MF, White DJ, 2003. Interface load transfer degradation during cyclic loading: a microscale investigation. *Soils and Foundations*, 43(4):81-93. https://doi.org/10.3208/sandf.43.4_81

Evgin E, Fakharian K, 1996. Effect of stress paths on the behaviour of sand-steel interfaces. *Canadian Geotechnical Journal*, 33(6):853-865. https://doi.org/10.1139/t96-116-336

Fakharian K, 1996. Three-Dimensional Monotonic and Cyclic Behaviour of Sand-Steel Interfaces: Testing and Modelling. PhD Thesis, University of Ottawa, Ottawa, Canada. https://doi.org/10.20381/ruor-16729

He PF, Ma W, Mu YH, et al., 2018. Study on freezing strength characteristics and formation mechanism of frozen soil-concrete interface. *Transactions of the Chinese Society of Agricultural Engineering*, 34(23):127-133 (in Chinese). https://doi.org/10.11975/j.issn.1002-6819.2018.23.015

Ji YJ, Jia K, Yu QH, et al., 2017. Direct shear tests of freezing strength at the interface between cast-in-situ concrete and frozen soil. *Journal of Glaciology and Geocryology*, 39(1):86-91. https://doi.org/10.7522/j.issn.1000-0240.2017.0011

Johnston IW, Lam TSK, Williams AF, 1987. Constant normal stiffness direct shear testing for socketed pile design in weak rock. *Géotechnique*, 37(1):83-89. https://doi.org/10.1680/geot.1987.37.1.83

Ko SG, Choi CH, 2011. Experimental study on adfreeze bond strength between frozen sand and aluminium with varying freezing temperature and vertical confining pressure. *Journal of the Korean Geotechnical Society*, 27(9):67-76. https://doi.org/10.7843/kgs.2011.27.9.067

Ladanyi B, 1995. Frozen soil-structure interfaces. *Studies in Applied Mechanics*, 42:3-33. https://doi.org/10.1016/S0922-5382(06)80004-8

Lashkari A, 2013. Prediction of the shaft resistance of nondisplacement piles in sand. *International Journal for Numerical and Analytical Methods in Geomechanics*, 37(8):904-931. https://doi.org/10.1002/nag.1129

Lee J, Kim Y, Choi C, 2013. A study for adfreeze bond strength developed between weathered granite soils and aluminum plate. *Journal of the Korean GEO-Environmental Society*, 14(12):23-30. https://doi.org/10.14481/jkges.2013.14.12.023

Mortara G, Mangiola A, Ghionna VN, 2007. Cyclic shear stress degradation and post-cyclic behaviour from sand-steel interface direct shear tests. *Canadian Geotechnical Journal*, 44(7):739-752. https://doi.org/10.1139/t07-019

Pan YM, Wang BX, Zhang ZQ, et al., 2022. Analysis on mechanical properties of thawing soil-concrete interface. *Journal of Henan Polytechnic University (Natural Science)*, 41(1):167-173 (in Chinese). https://doi.org/10.16186/j.cnki.1673-9787.2019080025

Peerun MI, Ong DEL, Choo CS, 2019. Interpretation of geomaterial behavior during shearing aided by PIV technology. *Journal of Materials in Civil Engineering*, 31(9):04019195. https://doi.org/10.1061/(ASCE)MT.1943-5533.0002834

Peerun MI, Ong DEL, Choo CS, et al., 2020. Effect of interparticle behavior on the development of soil arching in soil-structure interaction. *Tunnelling and Underground Space Technology*, 106:103610. https://doi.org/10.1016/j.tust.2020.103610

Puswewala UGA, 1991. Computational Modelling of Structure-Frozen Soil/Ice Interaction. PhD Thesis, University of Manitoba, Manitoba, Canada.

Roggensack WD, Morgenstern NR, 1978. Direct shear tests on natural fine-grained permafrost soils. Proceedings of the 3rd International Permafrost Conference, p.728-735.

Saberi M, Annan CD, Konrad JM, 2018a. On the mechanics and modeling of interfaces between granular soils and structural materials. *Archives of Civil and Mechanical Engineering*, 18(4):1562-1579. https://doi.org/10.1016/j.acme.2018.06.003

Saberi M, Annan CD, Konrad JM, 2018b. A unified constitutive model for simulating stress-path dependency of sandy and gravelly soil–structure interfaces. *International Journal of Non-Linear Mechanics*, 102:1-13. https://doi.org/10.1016/j.ijnonlinmec.2018.03.001

Shi QB, Yang P, 2021. Construction of statistical shear damage model at the interface between frozen fine sand and steel plate. *Journal of Railway Science and Engineering*, 18(10):2591-2599 (in Chinese). https://doi.org/10.19713/j.cnki.43-1423/u.T20201094

Shi S, Zhang F, Feng DC, et al., 2020. Experimental investigation on shear characteristics of ice–frozen clay interface. *Cold Regions Science and Technology*, 176:103090. https://doi.org/10.1016/j.coldregions.2020.103090

Sumitani D, Ueda Y, Ohrai T, 2007. Study on adfreeze shear strength of frozen sand along curved interface. *Journal of the Japanese Society of Snow and Ice*, 69(3):347-356. https://doi.org/10.5331/seppyo.69.347

Sun TC, Gao XJ, Liao YM, et al., 2021. Experimental study on adfreezing strength at the interface between silt and concrete. *Cold Regions Science and Technology*, 190:103346. https://doi.org/10.1016/j.coldregions.2021.103346

Sun ZH, Bian HB, Wang CY, et al., 2020. Significance analysis of factors of freezing strength between silty clay and concrete lining. *Journal of Glaciology and Geocryology*, 42(2):508-514. https://doi.org/10.7522/j.issn.1000-0240.2020.0050

Tabucanon JT, Airey DW, Poulos HG, 1995. Pile skin friction in sands from constant normal stiffness tests. *Geotechnical Testing Journal*, 18(3):350-364. https://doi.org/10.1520/GTJ11004J

Ueda Y, Moriuchi K, Ohrai T, 2004. Influence of normal stress on the adfreeze interface on adfreeze shear strength of frozen soil. *Journal of the Japanese Society of Snow and Ice*, 66(2):197-205. https://doi.org/10.5331/seppyo.66.197

Volokhov SS, 2003. Effect of freezing conditions on the shear strength of soils frozen together with materials. *Soil Mechanics and Foundation Engineering*, 40(6):233-238. https://doi.org/10.1023/B:SMAF.0000017575.19213.67

Wang RH, Wang W, Cheng YF, 2006. Model study of tensile bearing capacity of a single pile under frozen condition. *Journal of Glaciology and Geocryology*, 28(5):766-771 (in Chinese). https://doi.org/10.3969/j.issn.1000-0240.2006.05.021

Wang RS, Ong DEL, Peerun MI, et al., 2022. Influence of surface roughness and particle characteristics on soil–structure interactions: a state-of-the-art review. *Geosciences*, 12(4):145. https://doi.org/10.3390/geosciences12040145

Wen Z, Yu QH, Ma W, et al., 2013. Direct shear tests for mechanical characteristics of interface between Qinghai-Tibetan silt and fiberglass reinforced plastics. *Rock and Soil Mechanics*, 34(S2):45-50 (in Chinese). https://doi.org/10.16285/j.rsm.2013.s2.004

Zhang JW, Ma W, Wang DY, et al., 2008. In-situ experimental study of the bearing characteristics of cast-in-place bored pile in permafrost regions of the Tibetan Plateau. *Journal of Glaciology and Geocryology*, 30(3):482-487 (in Chinese).

Zhang Q, Zhang JM, Wang HL, et al., 2021. Mechanical behavior and constitutive relation of the interface between warm frozen silt and cemented soil. *Transportation Geotechnics*, 30:100624. https://doi.org/10.1016/j.trgeo.2021.100624

Zhou ZW, Ma W, Zhang SJ, et al., 2020. Experimental investigation of the path-dependent strength and deformation behaviours of frozen loess. *Engineering Geology*, 265: 105449. https://doi.org/10.1016/j.enggeo.2019.105449